

**LARGE- $t$  ELASTIC SCATTERING AND DIFFRACTION DISSOCIATION**

J. Timmermans,  
NIKHEF-H, Amsterdam, The Netherlands

ABSTRACT:

-----  
Recent results, both from the ISR and the  $S\bar{p}pS$  Collider, on proton-antiproton elastic scattering at large values of the four-momentum transfer squared, are presented. The results are compared with predictions of several theoretical models of high-energy collisions. Single diffraction dissociation at the Collider is also discussed.  
-----

### 1. Large- $t$ elastic scattering

The elastic and total cross sections and the differential cross sections for proton-proton and proton-antiproton scattering are very important quantities for the understanding of the dynamics of hadron-hadron interactions. Forward elastic scattering and total cross sections at very high energies have been treated in the talk by R. Castaldi at this Symposium. This paper will discuss the behaviour of the differential cross section at large values of the four-momentum transfer squared ( $-t \gtrsim 0.4 \text{ GeV}^2$ ).

High energy proton-proton scattering at large  $t$ -values has been extensively measured already several years ago at the ISR [1a,b]. These measurements were done at five different energies ( $\sqrt{s}=23, 31, 45, 53$  and  $62 \text{ GeV}$ ) up to  $-t=10 \text{ GeV}^2$  (at  $\sqrt{s}=53 \text{ GeV}$ ). The shapes of the distributions are characterized by a steep exponential decrease in the forward direction over about 7 orders of magnitude, reaching a rather sharp minimum at  $-t \approx 1.4 \text{ GeV}^2$  followed by a second maximum at  $-t \approx 1.8 \text{ GeV}^2$ , after which the cross section falls much slower with  $t$ . It is further observed that as energy increases, the forward diffraction peak shrinks, the minimum in the distribution moves to smaller  $|t|$  values and becomes less pronounced. No other dips are observed.

At much lower energies no dips are observed in the differential cross section distribution for proton-proton elastic scattering. Only a break of slope can be observed at  $-t \approx 1.5 \text{ GeV}^2$  [2]. It is only above  $p_{lab} \approx 150 \text{ GeV}/c$  that a diffractionlike dip structure becomes clearly visible [3a,b]. On the other hand, the differential cross section distribution for proton-antiproton elastic scattering shows already a sharp dip at the very low beam momenta of  $30 \text{ GeV}/c$  and  $50 \text{ GeV}/c$  [4]. While at the ISR the dip position was found to move inwards with increasing total cross section (i.e. increasing energy) as was expected from geometrical models, the dip in proton-antiproton elastic scattering at these low energies was moving outwards with increasing total cross section (i.e. decreasing energies). Very little energy dependence of the dip position was seen in  $p\bar{p}$  elastic scattering between  $p_{lab} = 50 \text{ GeV}/c$  and  $200 \text{ GeV}/c$  [3b].

The preliminary Collider results on  $p\bar{p}$  elastic scattering at large  $|t|$  [5] triggered a renewed interest, both theoretically and experimentally in high-energy, large  $|t|$  elastic scattering, and in particular the comparison between  $pp$  and  $p\bar{p}$  elastic scattering. Shortly before the closing down of the ISR, two experiments have measured large- $t$  elastic scattering both in  $p\bar{p}$  and  $pp$ , thus allowing a direct comparison of the differential cross section. The results will be given below. The UA4 experiment at the  $S\bar{p}pS$  Collider has acquired a much improved statistics and their final results are also presented.

---

The R608 experiment, a collaboration between CERN, Clermont-Ferrand, UCLA and Saclay, has recently published the results of a direct comparison of  $\bar{p}p$  and  $pp$  elastic scattering in the interval  $0.6 < -t < 2.1 \text{ GeV}^2$  at  $\sqrt{s}=53 \text{ GeV}$  [6]. The apparatus consisted of a magnetic spectrometer around the beam pipe on one side of the interaction point, measuring the momentum of the scattered  $\bar{p}$  ( $p$ ) in case of  $\bar{p}p$  ( $pp$ ) scattering and a set of scintillation counters around the beam pipe on the opposite side. Elastic events were selected through the momentum measurement of the  $\bar{p}$  ( $p$ ) together with a collinearity requirement on the directions of both scattered particles. Since the collinearity test could only be done in one projection, a sizeable background is still left, especially at large  $-t$  values (see Fig. 1). The numbers of elastic events have been determined from the collinearity distributions through a fit to a signal term + quadratic background. The resulting differential cross section distribution is shown in Fig. 2, both for  $pp$  (open circles) and  $\bar{p}p$  (solid circles). The curves are predictions by Donnachie and Landshoff [11], scaled up by 10% in order to have the same normalization as the data. These predictions will be discussed later. Within the limited statistics the  $\bar{p}p$  and  $pp$  measurements are found to be compatible.

The Ames-Bologna-CERN-Dortmund-Heidelberg-Warsaw Collaboration (R420) published last year already their results on a direct comparison of  $\bar{p}p$  and  $pp$  elastic scattering at three ISR energies  $\sqrt{s}=31, 53$  and  $62 \text{ GeV}$  up to  $-t=0.85 \text{ GeV}^2$  [7]. The experiment was performed using the Split Field Magnet (SFM) detector. Large samples of between 50,000 and 180,000 events remained at each energy after application of all the cuts. The resulting differential cross section distributions are shown in Fig. 3. Globally there is very little difference between the  $\bar{p}p$  and  $pp$  results. In the interval  $0.17 < -t < 0.85 \text{ GeV}^2$  all distributions are well represented by a simple exponential  $\sim \exp(bt)$ . The fit results for the slope parameter  $b$  are given in Table 1. The ratios of the  $\bar{p}p$  and  $pp$  differential cross sections have also been fitted to an exponential  $\sim \exp(\Delta bt)$ . The results of these fits are again given in Table 1. There may be still a slight difference in the slopes of the  $\bar{p}p$  and  $pp$  differential cross sections. However, the errors on the slope differences are large and it is thus not possible to infer an energy dependence of  $\Delta b$ .

New results at  $\sqrt{s}=53 \text{ GeV}$  have recently been presented by the R420 Collaboration, where now the  $t$ -range covered is  $0.5 < -t < 4.0 \text{ GeV}^2$  [8]. After all cuts 9834  $pp$  elastic scattering events and 1713  $\bar{p}p$  events were left. The  $pp$  differential cross section distribution is shown in Fig. 4 together with the high statistics results of an earlier experiment [1a]. The comparison above  $|t| = 0.8 \text{ GeV}^2$  shows good agreement between

the shapes of the two distributions. The normalization difference of 30% is within the estimated uncertainties of both experiments. The  $\bar{p}p$  differential cross section distribution of Fig. 5 however shows a different structure in the dip region when compared with the  $pp$  distribution. The authors conclude that the hypothesis of the  $\bar{p}p$  and  $pp$  differential cross sections being equal in the interval  $1.1 < -t < 1.5 \text{ GeV}^2$  is excluded at the 99.9% confidence level.

The UA4 Collaboration (Amsterdam, CERN, Genova, Napoli, Pisa) has now presented their final results on large- $t$  elastic scattering up to  $-t=1.55 \text{ GeV}^2$  at the CERN S $\bar{p}p$ S Collider [9]. The data were collected during the 1982 and 1983 Collider runs and represent an increase of statistics of about a factor five with respect to the data sample on which the preliminary results [5] were based. During these runs the Collider was operated in two different modes of the machine optics: the low- $\beta$  mode where the betatron functions at the interaction point take the values  $\beta_H=2\text{m}$  and  $\beta_V=1 \text{ m}$  in the horizontal and vertical planes respectively and the squeezed- $\beta$  mode with  $\beta_H=1.3 \text{ m}$  and  $\beta_V=0.65 \text{ m}$ . The average luminosity was about  $5 \times 10^{28} \text{ cm}^{-2}\text{s}^{-1}$ . In the vertical plane the size of the beams and their angular spread at the interaction point are  $\approx 0.1 \text{ mm}$  and  $\approx 0.15 \text{ mrad}$  respectively. The  $t$ -resolution, which is completely dominated by the angular beam spread, is given by  $\Delta t \approx 0.06 \sqrt{t}$  and is adequate to observe such a prominent dip-bump structure as is seen at the ISR in  $pp$  elastic scattering.

A schematic view of the apparatus is shown in Fig. 6a. Elastic events are observed by a system of sixteen detectors placed inside movable sections ("roman pots") of the vacuum chamber. Each detector consists of a scintillation counter hodoscope and a wire chamber. The wire chambers provide a point measurement with resolution of 0.07 mm and 0.4 mm in the vertical and horizontal coordinates respectively. The "pots" are arranged in two groups of four telescopes placed symmetrically with respect to the crossing point, above and below the machine plane. The outer telescopes are at a distance of about 40 m from the crossing point while the inner telescopes are at a distance of about 25 m. Each telescope is composed of two detectors that are 6 m and 3 m apart for the outer and inner telescopes respectively.

- Particles scattered in the crossing region traverse the quadrupoles  $Q_1$  and  $Q_2$  of the machine lattice before reaching the detectors. In the vertical plane  $Q_1$  produces a deflection by an angle of about  $2\Theta_V$  towards the beam axis, where  $\Theta_V$  is the vertical component of the scattering angle. The deflection of the quadrupole  $Q_2$  is approximately equal to  $\Theta_V$  (away from the beam axis).

- The trigger was provided by a left-right coincidence of the trigger counters in two opposite arms. It was an 8-fold coincidence during data taking in the squeezed- $\beta$  mode

---

and (due to the not complete left-right symmetry of the machine optics) a 6-fold coincidence in the low- $\beta$  mode. The deflection through the machine quadrupoles allowed a very powerful momentum selection. Particles coming from the crossing region with a momentum less than about 87% of the beam momentum were not accepted by the trigger (Fig. 7b). The momentum resolution of  $\Delta p/p = 0.006$  at  $p=273$  GeV/c is shown in Fig. 7a and is implicitly used in the analysis.

About 600,000 triggers were collected. The event selection was done according to the following steps:

- 1) In the track reconstruction procedure a hit was required in at least five out of the eight drift planes measuring the vertical coordinate and in at least one out of the two proportional wire planes, measuring the horizontal coordinate.
- 2) A single track was demanded in each telescope of two opposite arms without tracks in the other telescopes.
- 3) Events were rejected if a hit was present in a system of scintillation counter hodoscopes covering the pseudorapidity range  $2.5 \leq |\eta| \leq 5.6$  on both sides of the crossing point (see Fig. 6b).
- 4) A three-standard-deviation cut was applied to the distributions of the reconstructed vertical coordinate  $y_0$  of the proton and antiproton trajectories at the centre of the crossing region. Such a cut corresponds to a selection of events where the momentum of both the proton and the antiproton is within 2% of the beam momentum. The distributions of  $y_0$  for three different intervals of  $t$  are shown in Fig. 8. The amount of background seen is small, even at the largest values of the momentum transfer.
- 5) A three-standard-deviation cut was also applied to the distribution of the collinearity in the vertical plane:  $\Theta_V(\bar{p}) - \Theta_V(p)$ . The collinearity distributions for three  $t$  intervals are also shown in Fig. 8. A clear signal of elastic events can be seen with negligible background.
- 6) In order to ensure sufficient clearance inside the quadrupole vacuum chamber, the horizontal component of the scattering angle was limited to  $|\Theta_H| \leq 0.15$  mrad.

About 45,000 events were retained within the above cuts. The resulting differential cross section distribution is shown in Fig. 9. The absolute normalization is obtained by smoothly joining the present data to the earlier measurements below  $-t=0.5$  GeV<sup>2</sup> [10] and leads to an overall normalization error of 10%. No dip is observed in the distribution which shows an exponential decrease with momentum transfer and a break at  $-t \approx 0.9$  GeV<sup>2</sup> followed by a shoulder. Above  $-t=0.9$  GeV<sup>2</sup> the differential cross section is of the order of 1  $\mu\text{b}/\text{GeV}^2$  and decreases slowly with  $t$ .

The proton-proton elastic scattering data at ISR energies [1a] were fitted using a sum of two interfering amplitudes with exponential  $t$ -dependence:

$$d\sigma/dt \propto \left| e^{b(t-t_0)/2} + e^{d(t-t_0)/2+i\phi} \right|^2.$$

Complete destructive interference would occur at  $t=t_0$  if the relative phase  $\phi$  is equal to  $\pi$ . Also the present data are well represented by this parameterization. A fit in the range  $0.21 \leq -t \leq 1.55 \text{ GeV}^2$  gave the following results:

$$\begin{aligned} b &= 12.9 \pm 0.1 \text{ GeV}^{-2}, \\ d &= 2.4 \pm 0.2 \text{ GeV}^{-2}, \\ -t_0 &= 0.84 \pm 0.01 \text{ GeV}^2, \\ \phi &= \pi - (0.82 \pm 0.04), \end{aligned}$$

with a  $\chi^2=51$  for 56 degrees of freedom. The relatively large value of the phase difference  $\phi-\pi$  reflects the absence of a dip in the data.

A comparison between the Collider results on  $\bar{p}p$  elastic scattering at  $\sqrt{s}=546 \text{ GeV}$  and the most precise ISR data from both  $pp$  and  $\bar{p}p$  at  $\sqrt{s}=53 \text{ GeV}$  is shown in Fig. 10. There is a remarkable difference between the distributions at the two energies. One observes a persistent shrinkage with energy of the forward diffractive peak and the complete disappearance of the dip/second maximum structure which has developed into a shoulder. In addition the position of this structure moved to smaller values of  $|t|$  and the value of the differential cross section at the "second maximum" is more than one order of magnitude higher at the Collider than at ISR energies.

There exist several model predictions for the behaviour of the differential elastic cross section at large- $t$  values. A Regge type model by Donnachie-Landshoff [11] includes a three-gluon exchange contribution which, being odd under crossing, leads to the prediction of a dip in  $pp$  and the absence of a dip in  $\bar{p}p$ . Good fits were obtained to the ISR  $pp$  data. However the height of the shoulder predicted at the Collider is about one order of magnitude too low and the ISR  $\bar{p}p$  data seem to be below the prediction in the dip region. Reasonably good fits to the large- $t$  structures at low energies, at the ISR for  $pp$  and at the Collider could be obtained in the "nuclear core" model of Islam et al. [12]. They predicted also a sharp dip in  $\bar{p}p$  at the ISR at a smaller value of  $-t$  than for  $pp$ , which is in disagreement with the recent ISR results on  $\bar{p}p$  elastic scattering. In the geometrical scaling model of Dias de Deus and Kroll [13] the disappearance of the

---

dip can easily be accounted for by the growing real part of the forward elastic scattering amplitude. The model, which described well the energy dependence of the pp differential cross section in the dip region at the ISR, predicts too low by one order of magnitude the cross section in the shoulder seen at the Collider.

- A much stronger increase of the differential cross section with energy was already predicted several years ago by the factorizing eikonal type models [14] with increasing central blackness of the (anti)proton. In these models the scattering amplitude is written as an integral in impact parameter space over the profile function of the scattering hadrons. The eikonal in the profile function is then assumed to factorize into an energy dependent part and a function representing the hadronic matter distribution in impact parameter space. Since the original predictions of reference [14], which agree qualitatively with the present data from ISR and Collider, different parameterizations of the eikonal have been used in order to improve the qualitative agreement with the data [15]. Several of the above-mentioned predictions are shown in Fig. 10. It is clear that the eikonal models are favoured by the data. These models also predict that, as the total cross section rises with energy, the ratio of the elastic to total cross section should increase. This has indeed been observed at the Collider (see the talk by R. Castaldi at this Conference).

## II. Single diffraction dissociation at the Collider

The reaction  $\bar{p}p \rightarrow \bar{p}X$  was studied [16] by detecting the unfragmented antiproton as well as the charged decay products of the system X. Data were taken together with the large-t elastic data described in the previous section. The decay products of the system X are detected in the vertex detector shown in Fig. 6b. The detector consists of two identical systems of three telescopes  $D_1$ ,  $D_2$  and  $D_3$  placed symmetrically on the left and right side of the crossing region and covering angles from  $\sim 0.5^\circ$  to  $\sim 10^\circ$  corresponding to a range from 2.5 to 5.6 in the pseudorapidity variable  $\eta$ . Each telescope is composed of six drift chamber planes of full azimuthal coverage backed by a plane of trigger counters ( $T_1$ ,  $T_2$  and  $T_3$ ). The solid angle coverage of the apparatus is increased by the use of the UA2 central detector (CD) which covers the range  $-1.7 < \eta < 1.7$ . The scattered antiproton at small angles is observed in the telescope of "roman pot" detectors for the elastic scattering measurement.

The trigger required a particle through the two pot telescopes of either the upper or the lower arm on the  $\bar{p}$  side with at least one charged particle in the pseudorapidity range  $3 < \eta < 5.6$  in the opposite hemisphere. In addition, events with charged particles in

the range  $-5.6 < \eta < -4.4$  on the  $\bar{p}$  side were vetoed in order to make the trigger more selective against halo particles background.

The mass of the system X is calculated from  $M^2 = (1-x)s$  where  $x=p/p_0$ , the ratio of the measured antiproton momentum  $p$  and the beam momentum  $p_0$ . The resolution on the momentum and thus on  $x$  is 0.6%. The mass distribution of the system X is shown in Fig. 11 for two values of the square of the four-momentum transfer to the antiproton. The distributions clearly show the presence of the quasi-elastic peak for  $M^2/s \lesssim 0.03$  which is typical of the inelastic diffractive process. It can also be seen from the figures that the invariant differential cross section  $d^2\sigma/dt dx$  approximately scales for  $x \lesssim 0.99$  when compared to ISR data [17]. The  $1/M^2$  dependence of the mass distribution, expected if the mechanism of the triple pomeron graph is dominant, and already observed at the ISR [17] and Fermilab [18] extends up to Collider energies in the range  $0.01 < M^2/s < 0.04$  (Fig. 12).

To study the topology of the diffractive events, the  $\eta$ -distributions for different intervals of  $M$  are given in Fig. 13. Similar distributions were already shown at the 1984 Moriond Conference [19]. However, a slightly different trigger was used for the present distributions: it requires a  $\bar{p}$  detected in two pot telescopes and at least one charged particle in the range  $2.5 < \eta < 5.6$  in the opposite hemisphere, with no veto on the  $\bar{p}$  side. The new distributions contain less statistics, but the pseudorapidity interval between  $-1.7$  and  $+1.7$  is now covered by using also tracks reconstructed in the UA2 central detector. The widening of the  $\eta$ -distribution with increasing  $M$  is clearly observed. At large masses particles are emitted even in the same hemisphere of the unfragmented antiproton at larger and larger values of  $\eta$ . Such a behaviour excludes a fireball-type decay and rather favours a mechanism of multiperipheral kind.

#### Acknowledgements

I would like to thank the organizers of the Symposium for the generous hospitality extended to me during my stay at Tsukuba and J.G. Zweizig of the R608 Collaboration for a discussion on their results.

\* \*

---

R E F E R E N C E S

- [1a] E. Nagy et al., Nucl. Phys. B150 (1979) 221.
- [1b] A. Böhm et al., Phys. Lett. 49B (1974) 491.
  
- [2] J. Allaby et al., Nucl. Phys. B52 (1973) 316;  
Z. Asa'd et al., Phys. Lett. 128B (1983) 124.
  
- [3a] C. Akerlof et al., Phys. Rev. D14 (1976) 2864;  
G. Fidecaro et al., Nucl. Phys. B173 (1980) 513;  
G. Fidecaro et al., Phys. Lett. 105B (1981) 309;  
R. Rusack et al., Phys. Rev. Lett. 41 (1978) 1632.
- [3b] D. Kaplan et al., Phys. Rev. D26 (1982) 723;  
R. Rubinstein et al., Phys. Rev. D30 (1984) 1413.
  
- [4] Z. Asa'd et al., Phys. Lett. 108B (1982) 51;  
Z. Asa'd et al., Phys. Lett. 130B (1983) 335.
  
- [5] J. Timmermans, UA4 Collaboration, Proceedings of the Third Moriond Workshop, La Plagne 1983, p.35.
  
- [6] S. Erhan et al., Phys. Lett. 152B (1985) 131.
  
- [7] A. Breakstone et al., Nucl. Phys. B248 (1984) 253.
  
- [8] A. Breakstone et al., preprint CERN/EP 85-9, submitted to Phys. Rev. Lett.
  
- [9] M. Bozzo et al., UA4 Collaboration, preprint CERN/EP 85-31, submitted to Phys. Lett. B.
  
- [10] M. Bozzo et al., UA4 Collaboration, Phys. Lett. 147B (1984) 385.
  
- [11] A. Donnachie and P.V. Landshoff, Nucl. Phys. B231 (1984) 189.
  
- [12] M.M. Islam, T. Fearnley and J.P. Guillaud, Nuovo Cim. 81A (1984) 737.
  
- [13] J. Dias de Deus and P. Kroll, J. Phys. G. Nucl. Phys. 9 (1983) L81.

- [14] H. Cheng, J.K. Walker and T.T. Wu, Phys. Lett. 44B (1973) 97;  
T.T. Chou and C.N. Yang, Phys. Rev. D19 (1979) 3268.
  
  - [15] C. Bourrely, J. Soffer and T.T. Wu, Nucl. Phys. B247 (1984) 15;  
C. Chiu, Phys. Lett. 142B (1984) 309;  
R.J. Glauber and J. Velasco, Phys. Lett. 147B (1984) 380.
  
  - [16] M. Bozzo et al., UA4 Collaboration, Phys. Lett. 136B (1984) 217.
  
  - [17] M.G. Albrow et al., Nucl. Phys. B108 (1976) 1.
  
  - [18] D.S. Ayres et al., Phys. Rev. Lett. 37 (1976) 1724;  
R.L. Cool et al., Phys. Rev. Lett. 47 (1981) 701.
  
  - [19] C. Vannini, UA4 Collaboration, Proceedings of the Nineteenth Rencontre de  
Moriond, La Plagne, 1984, Vol. 2, p. 771.
  
  - [20] U. Amaldi et al., Phys. Lett. 66B (1977) 390;  
L. Baksay et al., Nucl. Phys. B141 (1978) 1;  
G. Barbiellini et al., Phys. Lett. 39B (1972) 663.
-

TABLE 1.

Fitted slope parameter  $b$  for  $pp$  and  $\bar{p}p$  elastic scattering and fitted slope difference  $\Delta b(\bar{p}p-pp)$  in the interval  $0.17 < -t < 0.85 \text{ GeV}^2$  from Ref.[ 7].

$\sqrt{s}$ (GeV)	$b$ ( $pp$ ) ( $\text{GeV}^{-2}$ )	$b$ ( $\bar{p}p$ ) ( $\text{GeV}^{-2}$ )	$\Delta b$ ( $\text{GeV}^{-2}$ )
31	$10.92 \pm 0.15$	$11.16 \pm 0.20$	$0.28 \pm 0.23$
53	$11.06 \pm 0.11$	$11.50 \pm 0.15$	$0.37 \pm 0.18$
62	$10.71 \pm 0.08$	$11.12 \pm 0.15$	$0.29 \pm 0.17$

FIGURE CAPTIONS

- Figure 1. Distributions in recoil-proton collinearity (R608 experiment [6]) for 8 different  $t$ -bins:  
0.6-0.7, 0.7-0.8, 0.8-0.9, 0.9-1.0, 1.0-1.2, 1.2-1.5, 1.5-1.8 and 1.8-2.1 GeV<sup>2</sup>; (a-h) for  $\bar{p}p$ , (i-p) for  $pp$ .
- Figure 2. Elastic  $d\sigma/dt$  for  $\bar{p}p$  and  $pp$  interactions [6]. The curves [11] are scaled up by 10% so that the  $pp$  curve is normalized to the data.
- Figure 3. Elastic differential cross sections at  $\sqrt{s}=31, 53$  and  $62$  GeV [7]. The 31 (53) GeV data have been scaled by a factor of 100 (10) for clarity.
- Figure 4. Elastic differential  $pp$  cross section at  $\sqrt{s}=53$  GeV [8]. Included are the low- $t$  data from ref.[7] and the  $pp$  data from ref.[1a].
- Figure 5. Elastic differential  $\bar{p}p$  cross section at  $\sqrt{s}=53$  GeV [8]. Included are the low- $t$  data from ref.[7] and the  $pp$  data from ref.[1a].
- Figure 6. a) Schematic view of one side of the UA4 elastic scattering lay-out at the Collider. The apparatus is symmetric with respect to the crossing point. The position of the detectors and of the machine quadrupoles is indicated. The trajectories in the vertical plane for the low- $\beta$  optics corresponding to a scattering angle of 2.5 mrad and for the high- $\beta$  optics (not discussed here) for an angle of 1.0 mrad are also shown.  
b) Lay-out of one arm of the UA4 inelastic detector. The set-up is symmetric with respect to the crossing point.
- Figure 7. a) The momentum resolution as determined from the analysis of elastic scattering events.  
b) The acceptance of the system for inelastically scattered (anti)protons for different values of  $t$  as a function of  $x$ , the ratio of the (anti)proton to the beam momentum.
- Figure 8. The vertical displacement of the antiproton and proton trajectories at the
-

centre of the crossing region,  $y_0(\bar{p})$  and  $y_0(p)$  respectively, are shown together with collinearity plots in the vertical plane. The upper, middle and lower section refer to the following three intervals of momentum transfer,  $0.55 \leq -t \leq 0.8 \text{ GeV}^2$ ,  $0.8 \leq -t \leq 1.2 \text{ GeV}^2$  and  $1.2 \leq -t \leq 1.55 \text{ GeV}^2$  respectively.

- Figure 9. The proton-antiproton differential cross section of elastic scattering at  $\sqrt{s}=546 \text{ GeV}$ . The measurements for  $-t \leq 0.5 \text{ GeV}^2$  [10] are also plotted. The rms  $t$ -resolution at  $-t=1 \text{ GeV}^2$  is  $0.06 \text{ GeV}^2$ .
- Figure 10. The  $\bar{p}p$  elastic scattering data at the  $S\bar{p}pS$  Collider ( $\sqrt{s}=546 \text{ GeV}$ ) compared to  $pp$  and  $\bar{p}p$  data at the ISR ( $\sqrt{s}=53 \text{ GeV}$ ) [1,7,8,20]. The curves are from several model predictions described in the text [11,13-15].
- Figure 11. The invariant cross section of proton-antiproton interactions at  $\sqrt{s}=546 \text{ GeV}$  for  $-t=0.55$  and  $0.75 \text{ GeV}^2$  is compared to the proton-proton data at ISR energies from ref.[17] at the same  $t$ -values.
- Figure 12. The non-invariant cross section  $d^2\sigma/dt dM^2$  at  $-t=0.55 \text{ GeV}^2$  is shown as a function of  $M^2$  together with proton-proton results from ref.[17]. Only data in the range  $0.01 < M^2/s < 0.04$  are displayed.
- Figure 13. Pseudorapidity distributions of diffractive events for different values of the mass  $M$  of the produced system.

\* \* \*

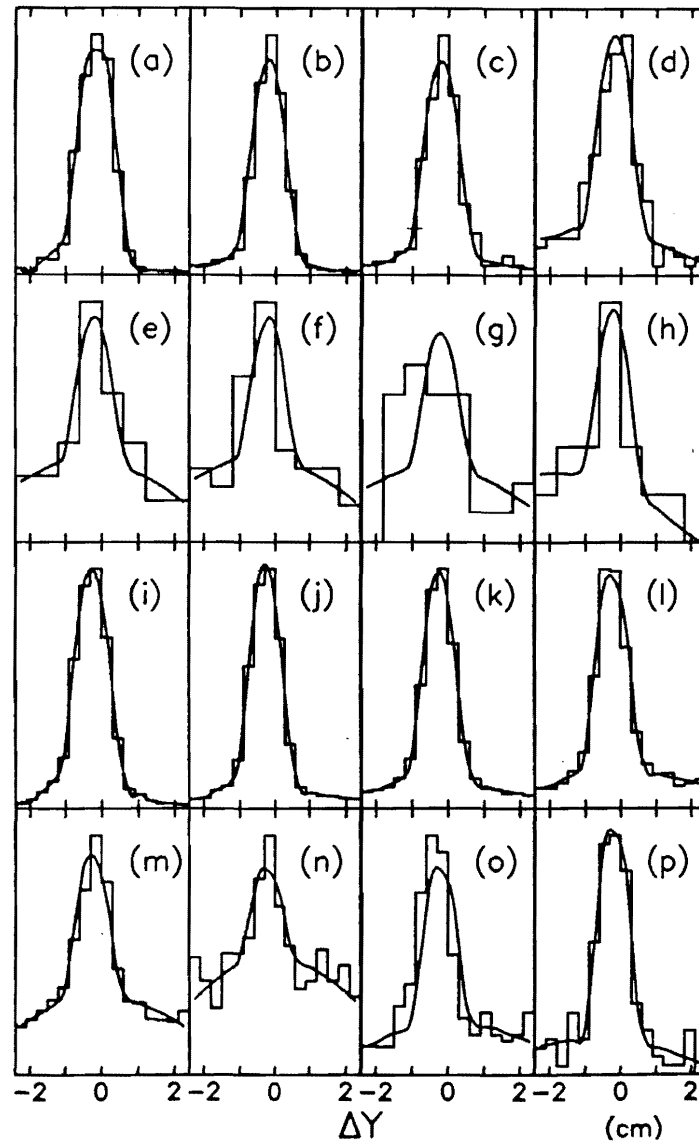


Figure 1

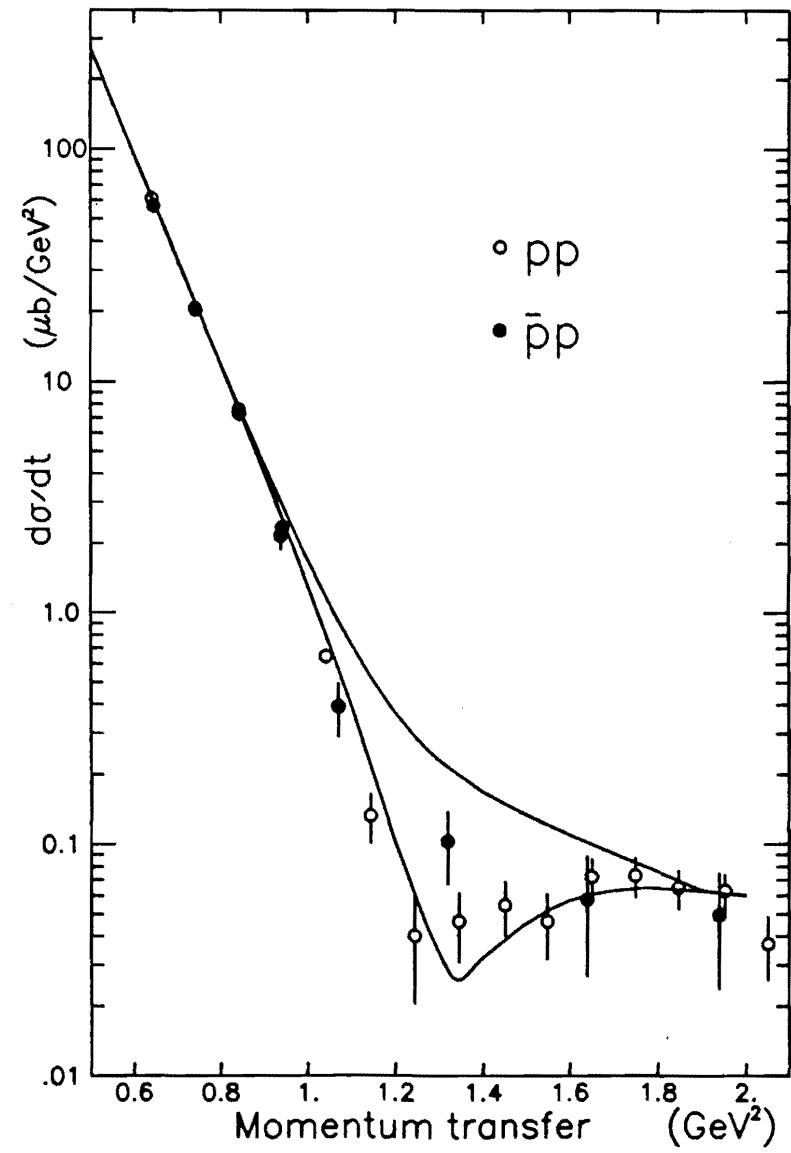


Figure 2

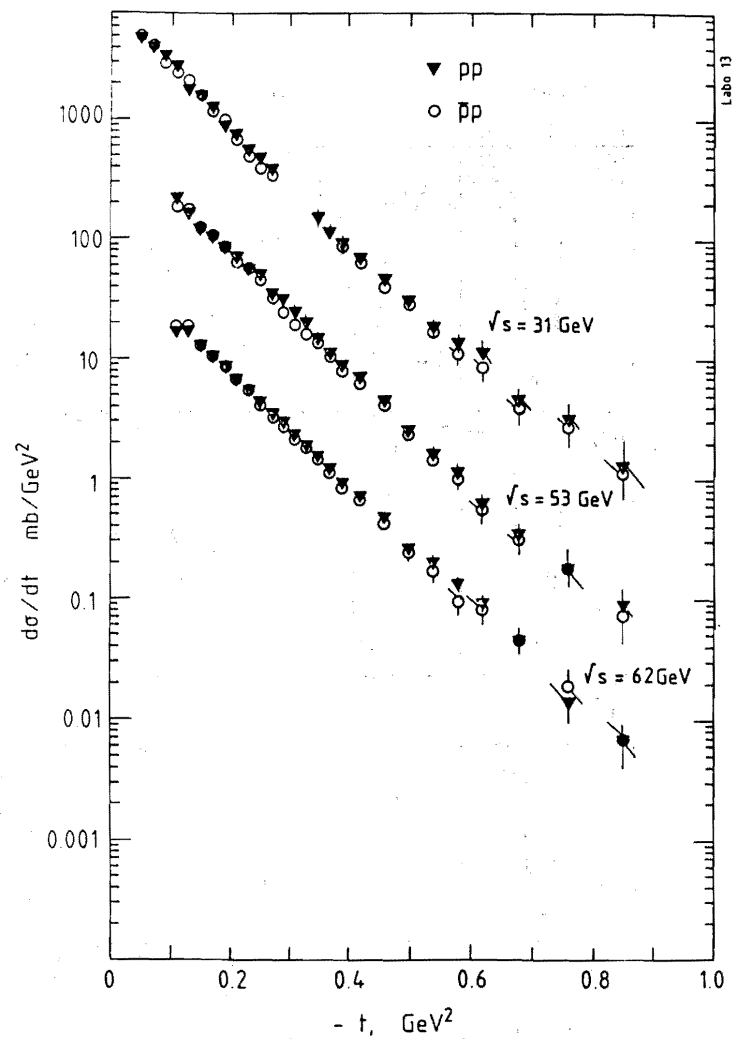


Figure 3

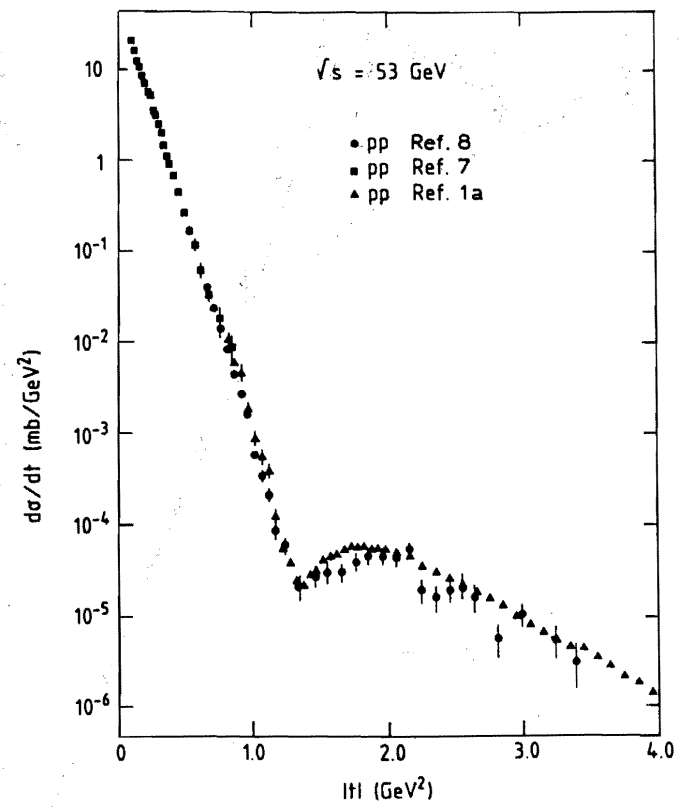


Figure 4

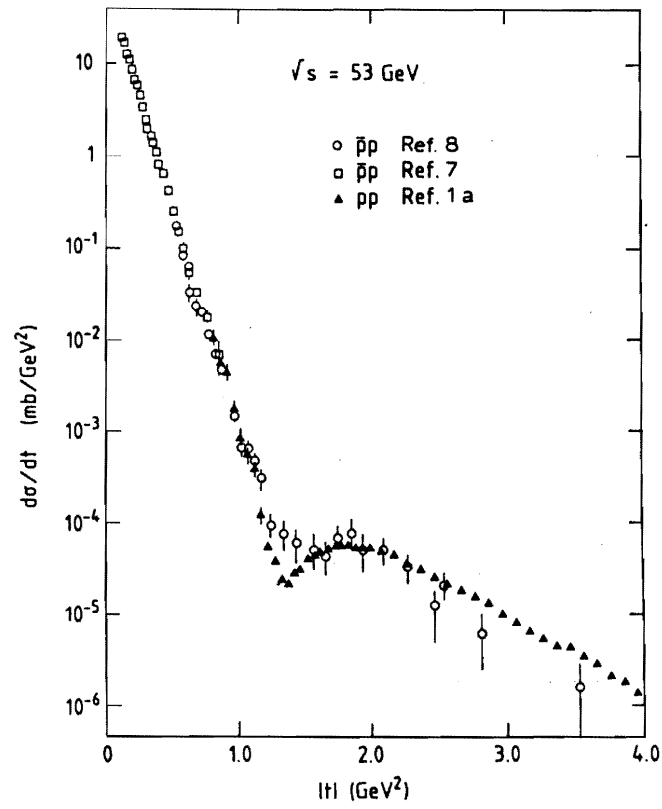


Figure 5

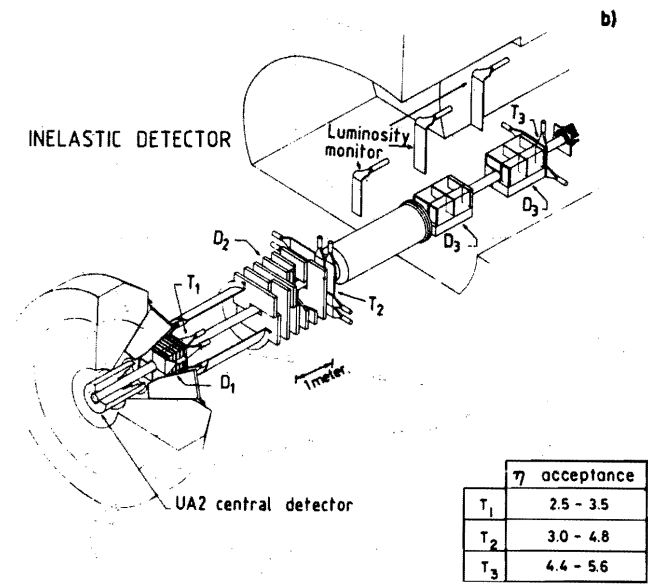
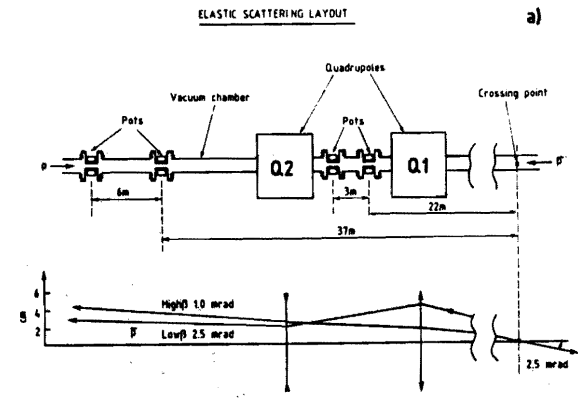


Figure 6

UA 4

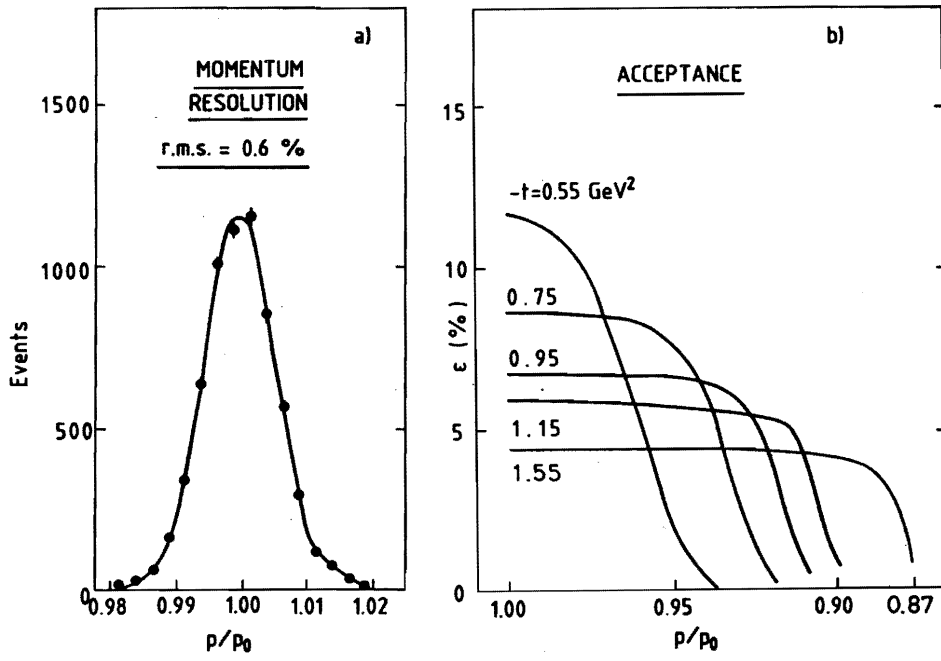


Figure 7

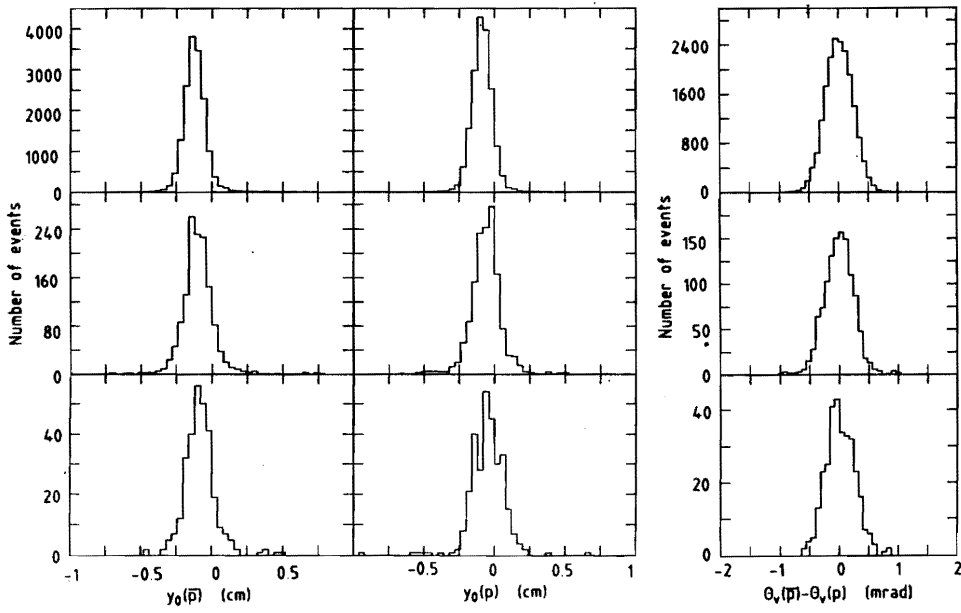


Figure 8

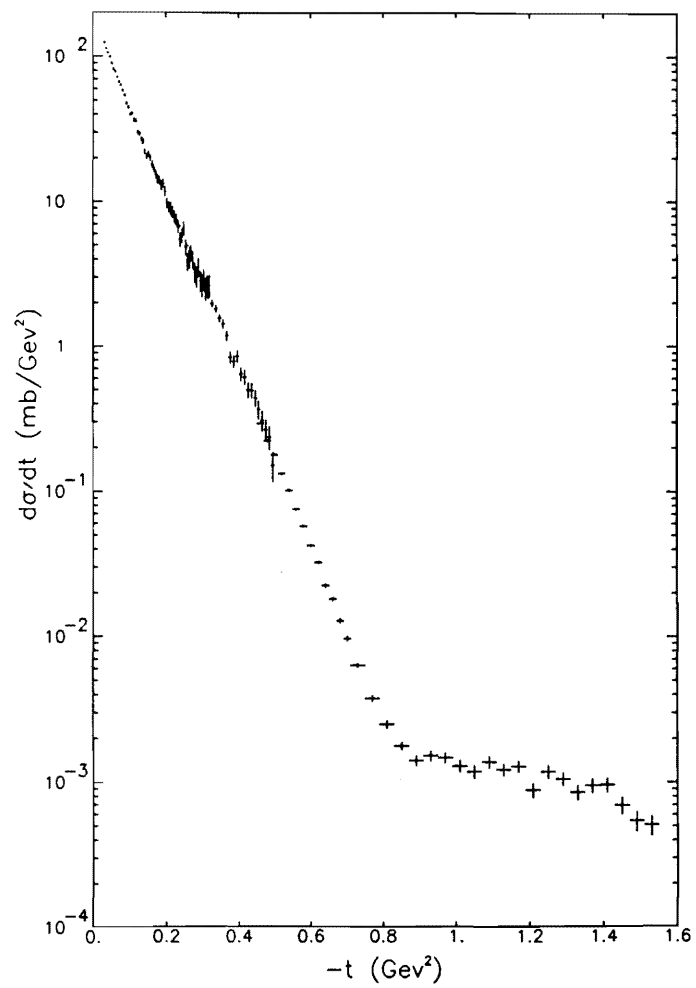


Figure 9

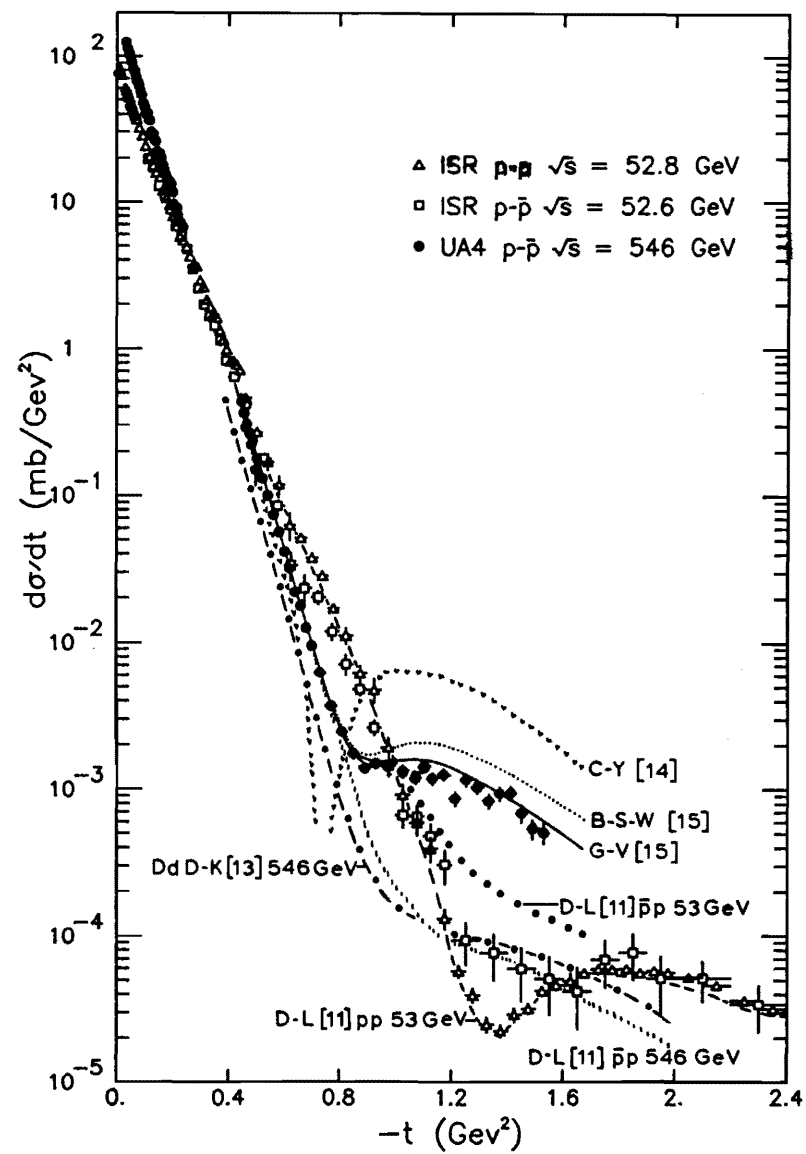


Figure 10

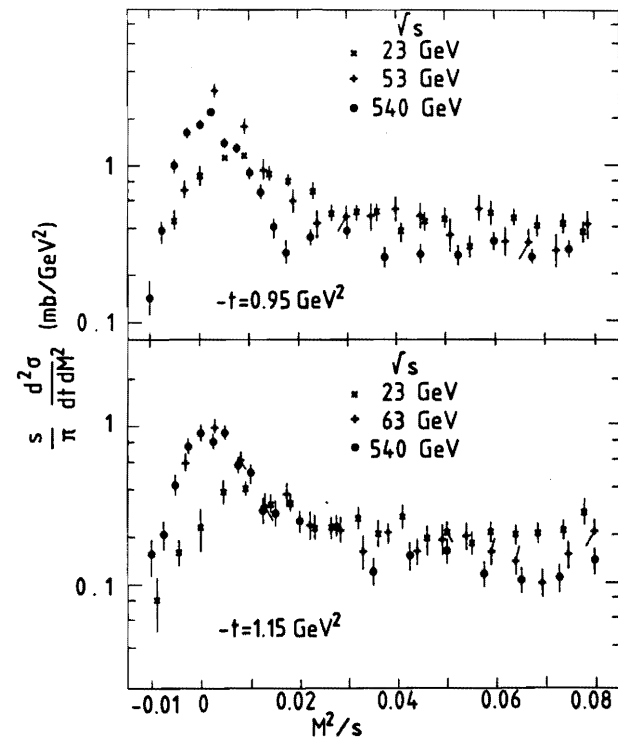


Figure 11

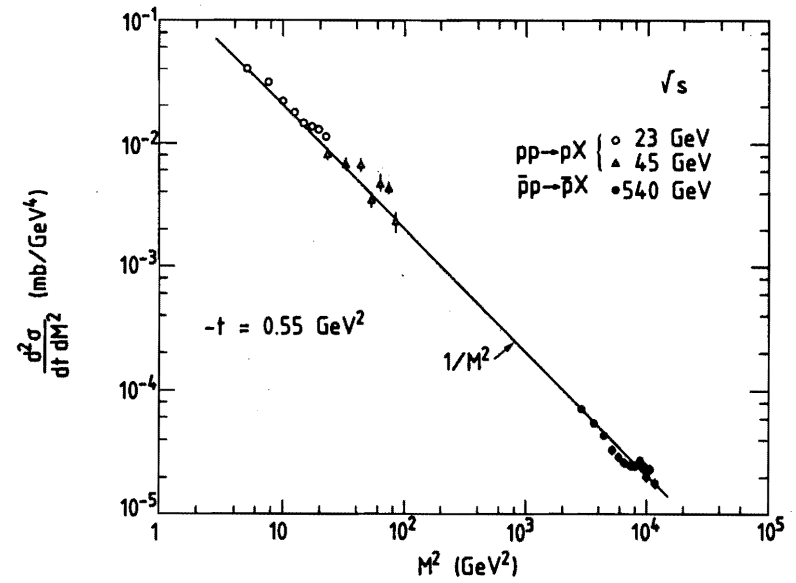


Figure 12

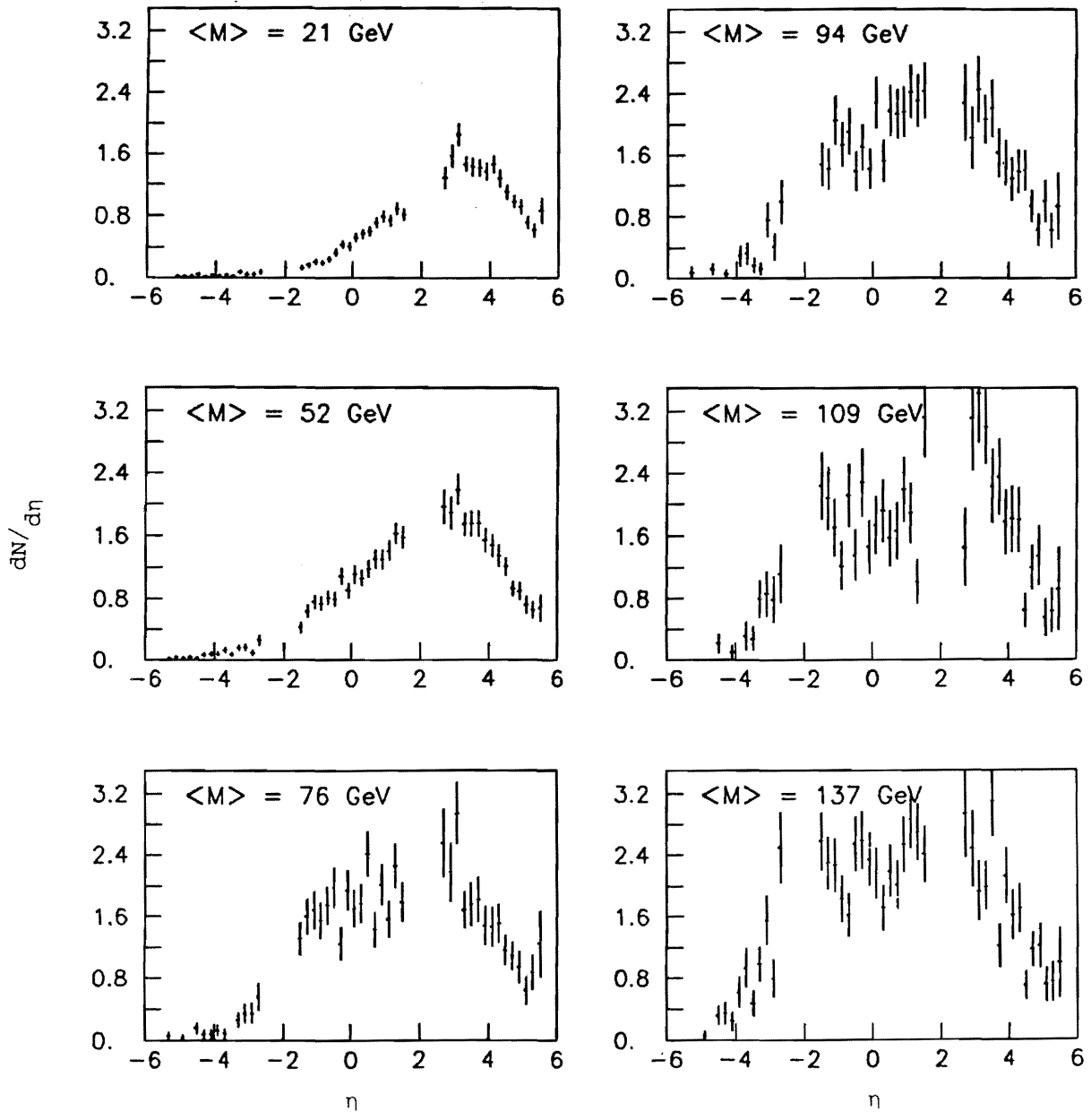


Figure 13